

# Scalable Functionalization of Optical Fibers Using Atomically Thin Semiconductors

Gia Quyet Ngo, Antony George,\* Robin Tristan Klaus Schock, Alessandro Tuniz, Emad Najafidehaghani, Ziyang Gan, Nils C. Geib, Tobias Bucher, Heiko Knopf, Sina Saravi, Christof Neumann, Tilman Lühder, Erik P. Schartner, Stephen C. Warren-Smith, Heike Ebendorff-Heidepriem, Thomas Pertsch, Markus A. Schmidt, Andrey Turchanin,\* and Falk Eilenberger\*

Atomically thin transition metal dichalcogenides are highly promising for integrated optoelectronic and photonic systems due to their exciton-driven linear and nonlinear interactions with light. Integrating them into optical fibers yields novel opportunities in optical communication, remote sensing, and all-fiber optoelectronics. However, the scalable and reproducible deposition of high-quality monolayers on optical fibers is a challenge. Here, the chemical vapor deposition of monolayer MoS<sub>2</sub> and WS<sub>2</sub> crystals on the core of microstructured exposed-core optical fibers and their interaction with the fibers' guided modes are reported. Two distinct application possibilities of 2D-functionalized waveguides to exemplify their potential are demonstrated. First, the excitonic 2D material photoluminescence is simultaneously excited and collected with the fiber modes, opening a novel route to remote sensing. Then it is shown that third-harmonic generation is modified by the highly localized nonlinear polarization of the monolayers, yielding a new avenue to tailor nonlinear optical processes in fibers. It is anticipated that the results may lead to significant advances in optical-fiber-based technologies.


This limitation reduces the total optical response of the TMDs and restricts possible applications severely. Therefore, strategies which enhance the light–matter interaction are highly desired. Coupling the TMDs with different types of optical resonators is a widely used method to enhance the light–matter interaction.<sup>[3–8]</sup> It is, however, naturally limited to narrowband resonances, while broadband, ultrafast operation cannot easily be implemented. On the other hand, by integrating TMDs on waveguides or optical fibers the interaction length can be enhanced greatly in a broadband, non-resonant manner.<sup>[9]</sup> The resulting 2D-functionalized waveguides (2DFWGs) can utilize the optical properties of TMDs via interaction with parts of the evanescent fields of the guided modes. 2DFWGs can show remarkable features, leveraging from, for example, the nonlinear or excitonic properties of the TMDs. Previous attempts to fabricate 2DFWG rely on mechanical transfer of exfoliated TMDs onto the waveguides or optical fibers.<sup>[10–14]</sup>

The light–matter interaction length in monolayer transition metal dichalcogenides (TMD)<sup>[1,2]</sup> on planar substrates is restricted to sub-nanometers due to their miniscule thickness.

The nonlinear or excitonic properties of the TMDs. Previous attempts to fabricate 2DFWG rely on mechanical transfer of exfoliated TMDs onto the waveguides or optical fibers.<sup>[10–14]</sup>

G. Q. Ngo, R. T. K. Schock, N. C. Geib, T. Bucher, H. Knopf, S. Saravi, Prof. T. Pertsch, Dr. F. Eilenberger  
Institute of Applied Physics  
Abbe Center of Photonics  
Friedrich Schiller University  
Albert-Einstein-Str. 15, Jena 07745, Germany  
E-mail: falk.eilenberger@uni-jena.de

Dr. A. George, E. Najafidehaghani, Z. Gan, Dr. C. Neumann, A. Turchanin  
Institute of Physical Chemistry  
Abbe Center of Photonics  
Friedrich Schiller University  
Lessingstr. 10, Jena 07743, Germany  
E-mail: antony.george@uni-jena.de; andrey.turchanin@uni-jena.de

 The ORCID identification number(s) for the author(s) of this article can be found under <https://doi.org/10.1002/adma.202003826>.

© 2020 The Authors. Published by Wiley-VCH GmbH. This is an open access article under the terms of the Creative Commons Attribution License, which permits use, distribution and reproduction in any medium, provided the original work is properly cited.

Dr. A. Tuniz  
University of Sydney Nano Institute (Sydney Nano)  
School of Physics  
Physics Road, Camperdown, NSW 2006, Australia  
H. Knopf, Prof. T. Pertsch, Dr. F. Eilenberger  
Fraunhofer-Institute for Applied Optics and Precision Engineering IOF  
Albert-Einstein-Str. 7, Jena 07745, Germany  
H. Knopf, Prof. T. Pertsch, Dr. F. Eilenberger  
Max Planck School of Photonics  
Jena 07745, Germany  
T. Lühder, Prof. M. A. Schmidt  
Leibniz Institute of Photonic Technology (IPHT)  
Albert-Einstein-Str. 9, Jena 07745, Germany  
Dr. E. P. Schartner, Dr. S. C. Warren-Smith,  
Prof. H. Ebendorff-Heidepriem  
ARC Centre of Excellence for Nanoscale BioPhotonics (CNBP)  
Institute for Photonics and Advanced Sensing  
School of Physical Sciences  
University of Adelaide  
Adelaide, SA 5005, Australia

DOI: 10.1002/adma.202003826

However, this approach is prone to induce uncontrollable stress fields and lacks reproducibility and scalability. Thus, such methods are hardly suitable for future large-scale integration. A process to grow high-quality monolayer TMDs directly on optical fibers or waveguides is therefore required to establish 2DFWGs as a new photonic platform. We tackle this challenge by directly growing monolayer TMDs on the guiding core of all-silica microstructured exposed-core optical fibers (ECFs),<sup>[15]</sup> a cross-sectional scanning electron microscopy (SEM) image of which can be found in Figure S2a,b, Supporting Information. Details on ECF-fabrication are given in the Experimental Section. The growth of 2D-materials turns the ECFs into 2DFWGs, in a scalable process. Specifically, we show the growth of monolayer MoS<sub>2</sub> and WS<sub>2</sub> crystals on the guiding core of all-silica ECFs and investigate their interaction with the evanescent fields of highly confined guided modes. The growth is facilitated by a modified chemical vapour deposition (CVD) process.<sup>[16]</sup> ECFs are compatible with this process, because they consist entirely of silica, which is a well-studied substrate material for high-temperature CVD processes and in particular for the growth of TMDs. The process yields interspersed monolayer TMD crystals of high quality with a typical length of 20 μm on ECFs with a length of a few centimeters. Our scalable technique paves the way for 2DFWGs as a new tool for integrated optical

architectures, active fiber networks, nonlinear light sources, distributed sensing, and photonic chips.

We highlight the possible functionalities of our 2DFWGs in two case studies. The first demonstrates in-fiber excitation and collection of exciton-driven photoluminescence (PL) which may pave ways toward future experiments in excitonics, remote fiber-based sensing schemes and surface-sensitive bio-analytics. The second is focused on how the highly nonlinear TMD coating modifies the nonlinear wave dynamics in ECFs, by investigating enhanced third-harmonic generation (THG). In general, this shows that 2DFWGs can be used to enhance and tailor the nonlinear response of integrated wave systems, leading to new applications in nonlinear light conversion and optical signal processing. The overall concept of both of our experiments is displayed in **Figure 1a**. The ECFs have been coated with MoS<sub>2</sub> and WS<sub>2</sub> crystals on the entire grooved surface, which also forms the upper surface of the ECFs core. A laser is coupled into the fundamental mode (FM) of the ECF, which interacts with the TMDs via the evanescent part of the mode. The resulting polarization, for example, PL or third-harmonic (TH) light, is coupled back into the fiber modes or into free space, where it can be collected for further analysis. An optical microscopy image of the coated exposed side of the ECF

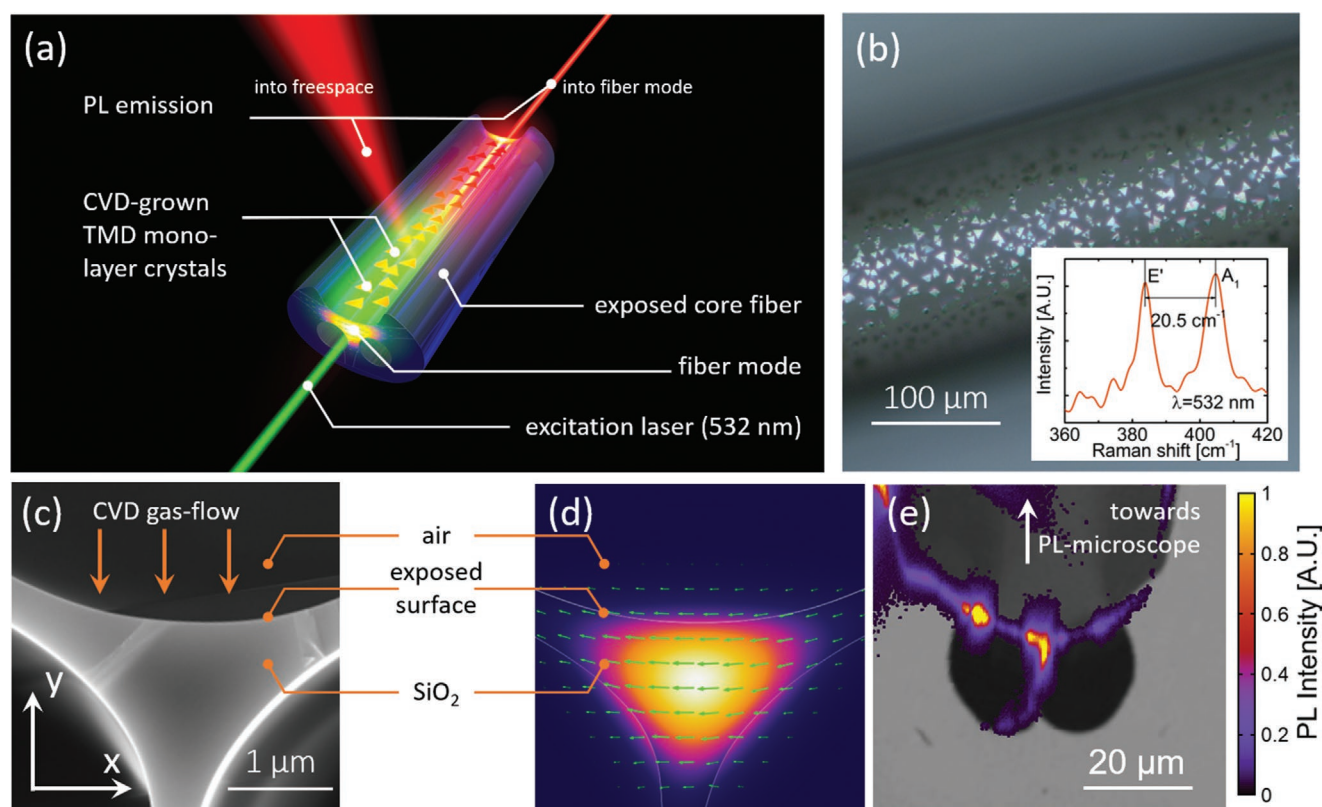


**Figure 1.** a) Artist's impression of a PL experiment with an ECF-based 2DFWG, where PL is excited with the fiber mode and is emitted into freespace and into the fiber mode which can be detected in either way. b) Optical microscopy image of the MoS<sub>2</sub>-coated ECF. The MoS<sub>2</sub> crystals on the exposed-core section of the fiber are clearly visible as bright triangles. The inset shows typical Raman spectrum of MoS<sub>2</sub> monolayer crystals grown on an ECF. c) Cross sectional SEM image of the core area of the ECF. Bright regions are SiO<sub>2</sub>, whereas dark regions are free of material. The gas flow on the CVD reactor is marked by orange arrows d) Simulated norm of the electric field distribution of the fundamental guided mode at 1570 nm. e) Cross sectional PL mapping of MoS<sub>2</sub>-coated ECF superimposed with a SEM image for clarification.

is given in Figure 1b, showing high-quality MoS<sub>2</sub> crystals. The focal plane of the image is chosen to coincide with bottom of the groove running along the entire 60 mm length of the coated ECF, which is also the top of the exposed core.

Figure 1c displays a cross sectional SEM image of the ECF's core area (an SEM image of the entire ECF cross section is provided in Figure S2a, Supporting Information). The core is suspended by three struts of silica to a homogenous silica cladding structure. The upper boundary of the core forms the bottom of a groove, which is running down the entire length of the ECF. When placed in the CVD reactor<sup>[16]</sup> the upper boundary of the core is thus completely exposed to the CVD reactants. Thus, as monolayer TMD crystals are grown on the entire outer surface of the ECF, they are also grown on the exposed upper surface of the core. Their lateral size, distribution and thickness can be tuned in the growth process. After careful optimization, monolayers were grown almost exclusively, as can be seen from the inset of Figure 1b, which displays a typical Raman spectrum of the MoS<sub>2</sub> crystals<sup>[17]</sup> on the ECF with a characteristic spacing of 20.5 cm<sup>-1</sup> between the Raman modes. This spacing is consistent with that expected for CVD-grown monolayer TMDs.<sup>[16,17]</sup> Examples of alternative growth modes together with their Raman spectra are displayed in Figure S2c–e. For more information on the growth process, please see the Experimental Section.

The ECF's core has a diameter of ≈2 μm and supports two nondegenerate FMs, which are mostly polarized along the *x* and *y* direction. However, the *x*-polarized FM, with the polarization aligned parallel to the coated surface, has a better field overlap with the TMD layer (see Table S1, Supporting Information) and its polarization is aligned with the large  $\chi_{xxxx}^{(3)}$ -components of the TMDs nonlinear tensor.<sup>[18]</sup> Hence, all experiments and simulations are carried out with the *x*-polarized FM. Its field distribution was calculated numerically (more details in Supporting Information) and is shown for a wavelength  $\lambda_0 = 1570$  nm in Figure 1d. Because of the small size of the core, the FM is well-confined. A fraction of 1.6% of the electromagnetic energy is flowing in the air region above the ECF's core, which can thus interact effectively with the TMD crystals.

Next, we verify the location and PL activity of the TMD crystals, grown on the curved ECF core by performing a cross

sectional PL emission mapping. The PL map displayed in Figure 1e is superimposed on a cross sectional SEM image of the ECF for easier understanding. Illumination and collection of PL light were performed sideways through the groove of the uncut ECF along the direction indicated by the arrow in Figure 1e. The PL follows the outline of the ECF groove, which indicates that the TMD crystals have grown in direct contact with the entire surface of the ECF. Note that the part of PL light extending downwards from the center of the image is caused by the diffraction at the ECF core and its interaction with the confocal setup and does not indicate the presence of TMDs within the core. A PL map along the propagation direction and a PL spectrum can be found in Figure S4, Supporting Information.

We now focus on guided wave excitation of PL in 2DFWGs, which is mediated by excitation and decay of excitons in the TMD coating. Excitons in TMDs<sup>[19]</sup> are particularly appealing because they exhibit spin valley coupling<sup>[20–23]</sup> and are important for the emission of single photons.<sup>[24–28]</sup> We couple a green laser ( $\lambda = 532$  nm) without polarization control into the ECF, which excites excitons via the evanescent field of the FM (for experimental setup see Figure S1, Supporting Information). PL from the TMD monolayers is either emitted into free space or coupled back into the ECF's mode. Emission into guided modes has been observed by imaging the end facet of the fiber and by measuring the spectrum. The results are displayed in Figure 2a,b. The image of the PL at the end facet of the ECF is long-pass filtered to remove residual laser radiation and then displayed in Figure 2a. For better orientation, a microscopy image of the ECF itself is superimposed. The PL light is clearly emitted from guided modes at the core of the ECF. This light is then analysed spectroscopically, revealing exciton peaks at 678 nm (MoS<sub>2</sub>) and 622 nm (WS<sub>2</sub>) and a spectral full-width at half-maximum of 48 and 43 nm, respectively. These values do not significantly differ from the ones reported on planar substrates grown by the same technique.<sup>[16]</sup> We thus conclude the material properties are comparable to those grown on planar substrates and no additional strain has been induced, e.g. due to different thermo-mechanical properties of the substrate.

Observing PL in the guided mode of the fiber means that the evanescent field of guided modes can be used to both excite and collect PL<sup>[29–31]</sup> in an integrated optical environment. This

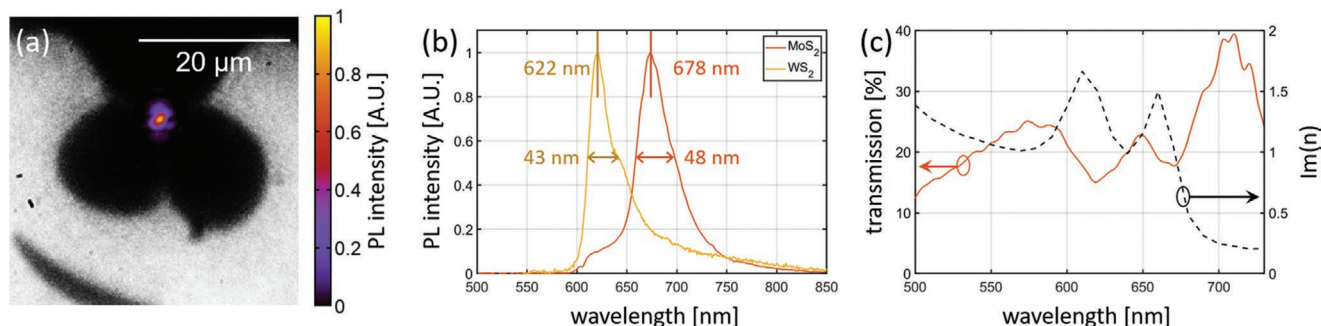


**Figure 2.** Modal PL and transmission measurement, where the laser/white light source is coupled into the TMD-coated ECF's guided mode and excites excitons in the TMD coating, which emit PL back into the fundamental mode. The PL signal is then recorded after it has propagated through the fiber. a) False-color image of PL excited by a 532 nm laser in a MoS<sub>2</sub>-coated ECF. The background image is the back surface of the ECF, recorded through the same camera. b) Normalized PL spectra of MoS<sub>2</sub>- and WS<sub>2</sub>-coated ECF excited by a 532 nm laser. c) Transmission spectrum through a MoS<sub>2</sub>-coated ECF. An LED white light source is used for transmission measurement. Values  $\lambda > 700$  nm are highly influenced by measurement inaccuracy, due to a lack of power of the light source for this spectral region.

makes 2DFWGs, such as TMD-coated ECFs, highly interesting for integrated excitonics and remote sensing applications.

Lateral emission into free space was observed with a camera mounted sideways, imaging the bottom of the ECFs groove. We attain compound images of the distribution of PL over a substantial section of the ECF and thus an image of PL active TMD crystals. One image such of a MoS<sub>2</sub>-coated fiber is displayed in Figure S5b, Supporting Information. From this, we can extract the distribution and cumulative length of monolayer crystals on the ECF. For this specific sample we observe 39 distinct MoS<sub>2</sub> crystals with an average length of 29 μm per crystal and a filling factor of 5.4%, although the coverage and crystal size have been significantly increased in later batches after further optimization of our growth procedure.

A transmission spectrum through the ECF is displayed in Figure 2c. It was obtained by coupling white light into the MoS<sub>2</sub>-coated ECF. This spectrum is shown with the imaginary part of the refractive index of MoS<sub>2</sub>, the two absorption peaks at 619 and 671 nm can thus be clearly connected to the characteristic exciton resonances the TMD.

2D TMDs are also highly interesting because of their strong nonlinear optical response per unit thickness.<sup>[32]</sup> For third order processes this is quantified by the nonlinear refractive index  $n_2$  with a reported value of  $n_2^{\text{MoS}_2} \approx 2.7 \times 10^{-16} \text{ m}^2 \text{ W}^{-1}$  for TMDs transferred on waveguides.<sup>[14]</sup> It is almost four orders of magnitude larger than that of silica, although lower values have been reported on planar substrates.<sup>[18]</sup> Thus, a TMD coating may have a substantial contribution to nonlinear effects in ECFs, although less than  $10^{-4}$  of the power flow of the FM is localized in the TMD at any wavelength (see Figure S6e, Supporting Information). The influence on the nonlinearity can be quantified by calculating the respective contributions of the MoS<sub>2</sub> coating and the SiO<sub>2</sub> core to the overall self-phase modulation coefficient  $\gamma = \gamma_{\text{MoS}_2} + \gamma_{\text{SiO}_2}$ .<sup>[33]</sup> Indeed, we find  $\gamma_{\text{MoS}_2} > \gamma_{\text{SiO}_2}$  for wavelength in excess of 1470 nm (see Section 7 (“Supplement 7: Fiber Nonlinearity, Self-Phase Modulation, and Third-Harmonic-Generation Coefficients”) and Figure S6g, Supporting Information), which means the nonlinear contribution of the TMD coating dominates for long wavelengths. Note, that even larger  $\gamma_{\text{MoS}_2}$  may be obtained in the future by optimizing the field overlap of the FM with the TMD coating, opening, for example, the path for TMD enhanced supercontinuum generation experiments.

While many third order nonlinear processes are observed in fibers, THG is particularly fascinating, because it relies on the simultaneous interplay of nonlinearity, mode matching, and phase matching (PM). We found that there is no appreciable modification of the PM by the TMD coating, because all linear mode properties, except loss, are unaffected by the TMD coating (see Figure S6, Supporting Information). The ECFs of the design used here, exhibit PM only for higher-order TH modes (HOMs) at a TH wavelength of roughly 550 nm, corresponding to a fundamental wavelength of 1650 nm.<sup>[34–36]</sup>

To show that THG is indeed enhanced we excited TH with a pulsed laser operating at  $\lambda_0 = 1570 \text{ nm}$  and a pulse duration of 32 fs (see Figure S7, Supporting Information for pulse characterization).<sup>[37]</sup> Figure 3a displays the TH spectrum for three different input energies for an uncoated and an MoS<sub>2</sub>-coated ECF. Measurements were qualitatively reproducible for individual ECFs but also across different samples. For ease of representation

we present data here from a representative sample. We consistently observe more THG in the MoS<sub>2</sub>-coated ECF, which signifies that the TMD coating does enhance the THG process. This is particularly noteworthy, as the MoS<sub>2</sub>-coated ECFs experience roughly 60% linear loss over the length of the ECF and the comparison was made for equal input energy. As dictated by PM we observe TH not at exactly a third of  $\lambda_0$  but in a spectral band ranging from 540 to 560 nm, marked in Figure 3a. The fundamental wave (FW) spectrum must thus first nonlinearly broaden (more details in Figure S8, Supporting Information) into a THG-relevant sub-band between 1620 to 1680 nm before TH is generated. This explains the somewhat stronger-than-cubic scaling in the inset Figure 3a. The similarity of TH spectrum for both ECF types reassures us that the phase matching (PM) between FW and TH is indeed unaffected by the MoS<sub>2</sub> coating.

Because a PM modification is thus ruled out, the observed TH enhancement must be related to the process of nonlinear light generation itself. This process is driven by the nonlinear polarization field  $\mathbf{P}^{\text{THG}} \left( \frac{\lambda_0}{3} \right) = E_x^3(x, y; \lambda_0) \cdot \chi_{xxxx}^{(3)}(x, y) \mathbf{e}_x$ . Here,  $E_x(x, y)$  is the x-component of the electric field of the FW mode and  $\chi_{xxxx}^{(3)}(x, y)$  is the dominating element of the nonlinear tensor of the THG process for the TMD coating and the silica core, respectively. The shape of  $\mathbf{P}^{\text{THG}}$  is displayed in Figure 3b in logarithmic scaling. There are two major contributions: the spatially smooth nonlinear polarization from the SiO<sub>2</sub> core and the strong but highly localized contribution of the TMD coating, better visible in the inset.

The so-generated TH radiation is distributed onto the TH modes, the magnitude of which is described by an overlap coefficient  $\gamma_k^{(\text{THG})}$  for every TH mode (see Supporting Information). Thus, the addition of the TMD coating does not enhance the nonlinear interaction for all HOMs equally but it boosts those that are localized close to the surface and with predominant x-polarization. This mode-selective nonlinear enhancement is quantified in Figure 3c, displaying  $\gamma_k^{(\text{THG})}$  values for all TH HOMs close to the PM point. The PM region contains 11 HOMs and is marked by the shading (see Supporting Information for determination of PM bandwidth  $\Delta n$ ). The contribution of SiO<sub>2</sub> and MoS<sub>2</sub> are marked in different colours. While  $\gamma_k^{(\text{THG})}$  grows for all HOMs, it does so very differently from mode, that is, the enhancement is mode-selective.

To confirm this model and to compare with the experiment, we only discuss the three HOMs with the largest  $\gamma_k^{(\text{THG})}$  marked with  $M_1$  to  $M_3$  in Figure 3c. The most dominant HOM is the  $M_1$  mode at  $n_{M_1}^{\text{eff}} = 1.379$ .  $\gamma_{M_1}^{(\text{THG})}$  is approximately doubled due to the MoS<sub>2</sub> coating. The second strongest contribution for the bare ECF comes from the  $M_2$  mode at  $n_{M_2}^{\text{eff}} = 1.366$ .  $\gamma_{M_2}^{(\text{THG})}$  increases by  $\approx 2.5$  upon application of the TMD coating. Upon coating; however, it is superseded by the  $M_3$  mode at  $n_{M_3}^{\text{eff}} = 1.383$ , which almost quadruples its  $\gamma_{M_3}^{(\text{THG})}$ . The modes profiles of  $M_1$ ,  $M_2$ , and  $M_3$  can be found in Figure S9, Supporting Information.

The mode-selective enhancement of the overlap coefficients is reflected in spatial distribution of the TH light as seen in images recorded by a camera, focused to output plane of the ECFs, displayed in Figure 3d,e for a bare and an MoS<sub>2</sub>-coated ECF of identical length, respectively. The single peak marked with the white oval at the top of the bare ECF is replaced by

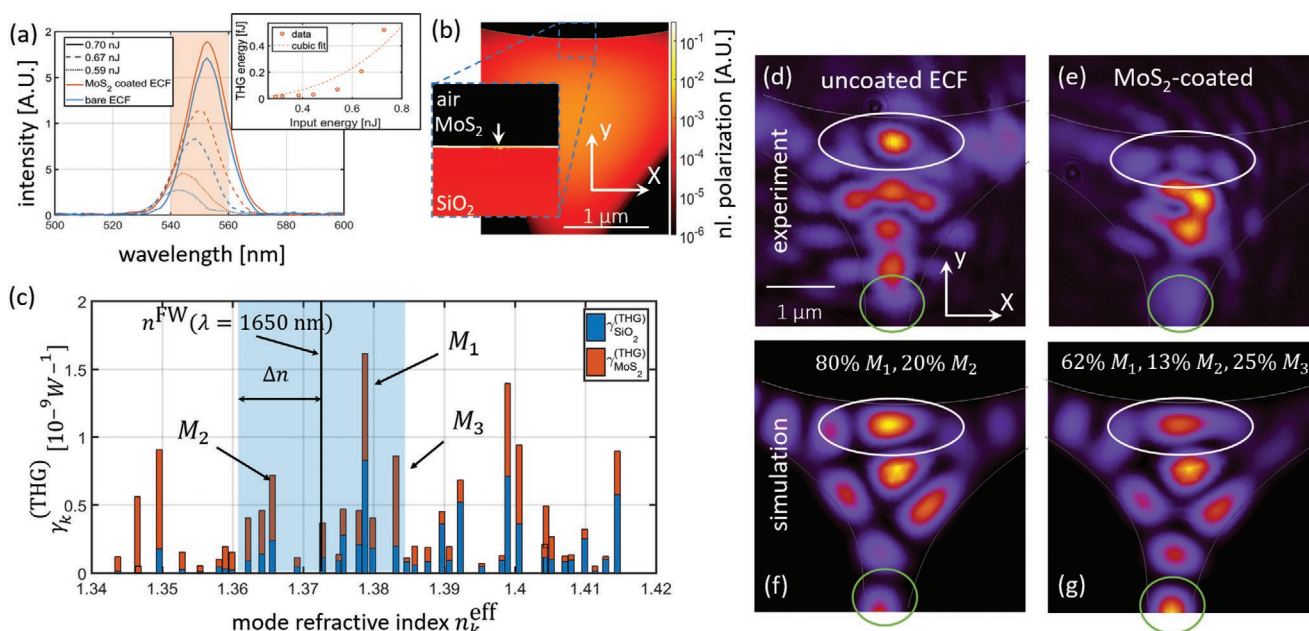


**Figure 3.** a) Third-harmonic spectra. The THG band from 540 to 560 nm is marked in orange. (Inset) Power dependence of the THG for the MoS<sub>2</sub>-coated ECF, with a cubic fit. b) Log-plot of the nonlinear polarization field, driving THG. The field is generated by the cubed FM and the nonlinear action of SiO<sub>2</sub> and MoS<sub>2</sub>. The inset is a zoom of the exposed surface, showing the strong and highly localized nonlinear polarization from the MoS<sub>2</sub>. c) Modal THG overlap coefficients  $\gamma_k^{(\text{THG})}$  at a TH wavelength of 550 nm, calculated for all HOMs  $k$ , which are close to the phase matching point at  $n_{\text{eff}}^{\text{FW}} = 1.373$ . The PM region with  $\Delta n < 0.012$  is marked in blue. The stacked colored bars mark the contributions of the SiO<sub>2</sub> core (blue) and the MoS<sub>2</sub> coating to  $\gamma_k^{(\text{THG})}$  (orange), respectively. d) Experimentally acquired image of the light distribution of the THG field at the end of a bare ECF. e) Experimentally acquired picture of the light distribution of the THG field at the end of a MoS<sub>2</sub>-coated ECF. f) Simulated picture at the end of the ECF as a superposition the  $M_1$  and  $M_2$ , with an 80/20 power distribution, according roughly to the overlap coefficients for the bare ECF. g) Simulated picture at the end of the ECF as a superposition the  $M_1$ ,  $M_2$  and  $M_3$ , according to a 62/13/25 power distribution according roughly to the overlap coefficients for the MoS<sub>2</sub>-coated ECF. In (d)–(g), the white ovals and green circles mark regions, in which the coated and uncoated ECF show appreciable differences.

a broader and weaker triple peaked distribution for the MoS<sub>2</sub>-coated ECF. Moreover, the field is less localized and extends further into the bottom strut for the MoS<sub>2</sub>-coated ECF in the region marked with the green circle. Qualitatively, both distributions can be reproduced by a simple superposition of the  $M_1$ ,  $M_2$  and  $M_3$  modes, displayed in Figure 3f,g, where the superposition coefficients are chosen according to the relative values of the overlap coefficients  $\gamma_{M_{1-3}}^{(\text{THG})}$  with and without the MoS<sub>2</sub> coating. Both the modifications at the top and bottom of the image are well-reproduced for such a simple model, particularly in light of the large uncertainties of the linear and nonlinear coefficients of MoS<sub>2</sub> and the impact of the random distribution of the crystals on the ECF.

In summary, we have shown that high-quality crystalline monolayer TMDs, for example, MoS<sub>2</sub> and WS<sub>2</sub>, can be grown directly on the core of microstructured exposed-core fibers in a scalable CVD process. This process functionalizes the optical fibers, creating a new platform to investigate and utilize the optoelectronic properties of 2D TMDs. Excitonic and nonlinear functionalization is demonstrated in two case studies. First, we excite and collect excitonic photoluminescence from monolayers in the optical fiber, which may give access to, for example, remote sensing schemes, leveraging on the sensitivity of the TMD excitons to the environment. Moreover, it may provide a new platform to investigate excitonic effects over long interaction lengths. A connection with in-fiber electrodes could be used to facilitate novel ultrafast detectors for light. We have

also demonstrated that 2D materials modify nonlinear optical processes intricately by investigating the enhancement of third-harmonic generation, which is found to be highly mode selective. This may well enhance the design freedom for highly nonlinear guided wave systems and may be utilized in nonlinear fiber devices. Altogether the direct growth of 2D materials on waveguides is opening a novel path toward the scalable and reproducible functionalization of waveguides, fibers, and other integrated optical systems.

## Experimental Section

**ECF Fabrication:** The fused silica ECF was fabricated using an ultrasonic drilled silica preform that was then cut open on one side to expose one part of the central section of the fiber. The preform was then caned and inserted into a jacket tube, which is then drawn into an ECF. Active pressurization was used during the draw on the central cane piece, to stabilize the structure.<sup>[15]</sup> The fiber has an outer diameter of 220  $\mu\text{m}$  (see Figure S2a, Supporting Information) and an effective core diameter of 2  $\mu\text{m}$ .

**CVD Growth of TMDs on Fibers:** MoS<sub>2</sub> and WS<sub>2</sub> crystals were grown on the ECF (fixed on a quartz holder) by a modified CVD growth method in which a Knudsen-type effusion cell is used for the delivery of sulfur precursor<sup>[16]</sup> from sulfur-powder and metal-oxide powder is used to supply the transition metal. Details of the method are given in ref. [16], from which no modifications were made, except for the usage of ECFs as the substrate. The grown TMDs on the ECFs were initially characterized using optical microscopy (Zeiss Axio Imager Z1.m) and Raman

spectroscopy (Bruker Senterra spectrometer operated in backscattering mode using 532 nm wavelength obtained with a frequency doubled Nd:YAG Laser, a 100× objective and a thermoelectrically cooled CCD detector).

**Microscopic PL Mapping and Spectroscopy:** Photoluminescence mapping was carried out with a commercial confocal PL lifetime microscope (Picoquant Microtime 200), with an excitation laser operating at 532 nm. The maps were created by moving the sample along the focus of the microscope's objective, which had a magnification of 64×. The resulting spatial resolution is estimated to be in the range of 500 nm. Detection of the PL signal was carried out with an avalanche photodiode. Alternatively, the PL microscope was connected to a grating spectrometer (Horiba Jobin Yvon Triax) equipped with a cooled CCD detector to measure PL spectra.

**In-Fiber and Transverse PL Mapping and Spectroscopy:** To record PL and transmission spectra, the incoming light was focused into the fiber core. For PL spectroscopy the outgoing light was passed through two 550 nm long-pass filters and then imaged into a spectrometer (Horiba Jobin Yvon Triax), with a cooled Si-CCD-detector. PL was excited with a 532 nm laser (Lighthouse Photonics Sprout), whereas transmission spectra were excited with a white light diode. Alternatively, the light was imaged onto a CMOS camera (Zyla 4.2 sCMOS), to image the PL at the output facet. The camera was alternatively mounted laterally together with a 10× objective imaging the sideways emission of PL from these crystals. Again, a set of 550 nm long-pass filters was used to reject scattered light from the excitation laser. The camera and the objective had been mounted on a motion stage to map larger sections of the fiber side.

**THG Measurements:** Nonlinear experiments were carried out with a femtosecond laser emitting pulses with a duration of 32 fs at a central wavelength of 1570 nm at a repetition rate of 80 MHz (Toptica FemtoFiber pro IRS-II) and focused into the ECF with an aspheric lens. Light leaving the fiber was collimated with a microscope objective and coupled into an optical spectrum analyser, to measure the FW and the TH spectra.

## Supporting Information

Supporting Information is available from the Wiley Online Library or from the author.

## Acknowledgements

F.E. was supported by the Federal Ministry of Education and Science of Germany under Grant ID 13XP5053A. Q.G.N., E.N., and S.S. are supported by the European Union, the European Social Funds and the Federal State of Thuringia as FGR 0088 under Grant ID 2018FGR00088 and FGR 0067, respectively. S.S. is also funded through the IMPULSE junior researcher promotion program of the Friedrich Schiller University Jena. N.C.G. and A.G. were supported by the German Research Council as part of the CRC SFB 1375 NOA project B3 and B2. This project received funding from the joint European Union's Horizon 2020 and DFG research and innovation programme FLAG-ERA under a Grant TU149/9-1. T.L. and M.S. acknowledge financial support from the German research foundation via the grants SCHM2655/9-1 and SCHM2655/11-1. A.T. is the recipient of an Australian Research Council Discovery Early Career Award (project number DE200101041) funded by the Australian Government. This work was performed in part at the OptoFab node of the Australian National Fabrication Facility utilizing Commonwealth and SA State Government funding. The authors thank Stephanie Höppener and Ulrich S. Schubert for enabling their Raman Spectroscopy studies at the JCSM.

Open access funding enabled and organized by Projekt DEAL.

Note: The first names and surname of author Robin Tristan Klaus Schock were misidentified in the originally published version. This was corrected on November 24, 2020, after initial publication online.

## Conflict of Interest

The authors declare no conflict of interest.

## Author Contributions

F.E. was the principal contributor to the manuscript and the overall coordinator of the experiments. A.G., M.A.S., A.T., A.Tur., and F.E. developed the concept and contributed to the overall course of the research. G.Q.N. conducted experiments and simulations for both case studies and was supported by R.T.K.S. A.G. developed the CVD process and adapted it for the ECFs. A.Tun. and S.S. supported the modelling of the nonlinear interaction coefficients. E.N., Z.G., and C.N. were responsible for material growth and structural characterization. N.C.G., T.B., H.K., and T.L. were responsible for optical materials characterization and characterization of the optical experiments. E.S., S.W.S., and H.E.H. developed the ECFs fabrication technique, provided samples and supported in the modelling of mode properties. All authors contributed to the manuscript.

## Keywords

2D materials, excitonic photoluminescence, integrated photonics, nonlinear optics, transition metal dichalcogenides

Received: June 4, 2020  
Revised: August 7, 2020  
Published online: October 6, 2020

- [1] K. F. Mak, C. Lee, J. Hone, J. Shan, T. F. Heinz, *Phys. Rev. Lett.* **2010**, *105*, 136805.
- [2] K. F. Mak, J. Shan, *Nat. Photonics* **2016**, *10*, 216.
- [3] T. Bucher, A. Vaskin, R. Mupparapu, F. J. F. Löchner, A. George, K. E. Chong, S. Fasold, C. Neumann, D.-Y. Choi, F. Eilenberger, F. Setzpfandt, Y. S. Kivshar, T. Pertsch, A. Turchanin, I. Staude, *ACS Photonics* **2019**, *6*, 1002.
- [4] S. Dufferwiel, S. Schwarz, F. Withers, A. Trichet, F. Li, M. Sich, O. Del Pozo-Zamudio, C. Clark, A. Nalitov, D. Solnyshkov, *Nat. Commun.* **2015**, *6*, 8579.
- [5] H. Knopf, N. Lundt, T. Bucher, S. Höfling, S. Tongay, T. Taniguchi, K. Watanabe, I. Staude, U. Schulz, C. Schneider, F. Eilenberger, *Opt. Mater. Express* **2019**, *9*, 598.
- [6] X. Liu, T. Galfsky, Z. Sun, F. Xia, *Nat. Photonics* **2015**, *9*, 30.
- [7] S. Wu, S. Buckley, J. R. Schaibley, L. Feng, J. Yan, D. G. Mandrus, F. Hatami, W. Yao, J. Vuckovic, A. Majumdar, *Nature* **2015**, *520*, 69.
- [8] Y. Ye, Z. J. Wong, X. Lu, X. Ni, H. Zhu, X. Chen, Y. Wang, X. Zhang, *Nat. Photonics* **2015**, *9*, 733.
- [9] X. Liu, Q. Guo, J. Qiu, *Adv. Mater.* **2017**, *29*, 1605886.
- [10] H. Chen, V. Corbolio, A. S. Solntsev, D.-Y. Choi, M. A. Vincenti, D. De Ceglia, C. De Angelis, Y. Lu, D. N. Neshev, *Light: Sci. Appl.* **2017**, *6*, e17060.
- [11] I. Datta, S. H. Chae, G. R. Bhatt, M. A. Tadayon, B. Li, Y. Yu, C. Park, J. Park, L. Cao, D. Basov, *Nat. Photonics* **2020**, *14*, 256.
- [12] L. Liu, K. Xu, X. Wan, J. Xu, C. Y. Wong, H. K. Tsang, *Photonics. Res.* **2015**, *3*, 206.
- [13] H. Zhang, N. Healy, A. F. J. Runge, C. C. Huang, D. W. Hewak, A. C. Peacock, *Opt. Lett.* **2018**, *43*, 3100.
- [14] Y. Zhang, L. Tao, D. Yi, J.-B. Xu, H. K. Tsang, *J. Opt.* **2020**, *22*, 025503.
- [15] E. P. Scharfner, A. Dowler, H. Ebendorff-Heidepriem, *Opt. Mater. Express* **2017**, *7*, 1496.
- [16] A. George, C. Neumann, D. Kaiser, R. Mupparapu, T. Lehnert, U. Hübner, Z. Tang, A. Winter, U. Kaiser, I. Staude, A. Turchanin, *J. Phys. Mater.* **2019**, *2*, 016001.

- [17] C. Lee, H. Yan, L. E. Brus, T. F. Heinz, J. Hone, S. Ryu, *ACS Nano* **2010**, *4*, 2695.
- [18] A. Säynätjoki, L. Karvonen, H. Rostami, A. Autere, S. Mehravar, A. Lombardo, R. A. Norwood, T. Hasan, N. Peyghambarian, H. Lipsanen, K. Kieu, A. C. Ferrari, M. Polini, Z. Sun, *Nat. Commun.* **2017**, *8*, 893.
- [19] A. Splendiani, L. Sun, Y. Zhang, T. Li, J. Kim, C.-Y. Chim, G. Galli, F. Wang, *Nano Lett.* **2010**, *10*, 1271.
- [20] T. Cao, G. Wang, W. Han, H. Ye, C. Zhu, J. Shi, Q. Niu, P. Tan, E. Wang, B. Liu, J. Feng, *Nat. Commun.* **2012**, *3*, 887.
- [21] K. F. Mak, K. He, J. Shan, T. F. Heinz, *Nat. Nanotechnol.* **2012**, *7*, 494.
- [22] G. Sallen, L. Bouet, X. Marie, G. Wang, C. R. Zhu, W. P. Han, Y. Lu, P. H. Tan, T. Amand, B. L. Liu, B. Urbaszek, *Phys. Rev. B* **2012**, *86*, 081301.
- [23] D. Xiao, G.-B. Liu, W. Feng, X. Xu, W. Yao, *Phys. Rev. Lett.* **2012**, *108*, 196802.
- [24] C. Chakraborty, L. Kinnischtzke, K. M. Goodfellow, R. Beams, A. N. Vamivakas, *Nat. Nanotechnol.* **2015**, *10*, 507.
- [25] Y.-M. He, G. Clark, J. R. Schaibley, Y. He, M.-C. Chen, Y.-J. Wei, X. Ding, Q. Zhang, W. Yao, X. Xu, C.-Y. Lu, J.-W. Pan, *Nat. Nanotechnol.* **2015**, *10*, 497.
- [26] M. Koperski, K. Nogajewski, A. Arora, V. Cherkez, P. Mallet, J.-Y. Veuillen, J. Marcus, P. Kossacki, M. Potemski, *Nat. Nanotechnol.* **2015**, *10*, 503.
- [27] A. Srivastava, M. Sidler, A. V. Allain, D. S. Lembke, A. Kis, A. Imamoglu, *Nat. Nanotechnol.* **2015**, *10*, 491.
- [28] P. Tonndorf, R. Schmidt, R. Schneider, J. Kern, M. Buscema, G. A. Steele, A. Castellanos-Gomez, H. S. J. van der Zant, S. M. de Vasconcellos, R. Bratschitsch, *Optica* **2015**, *2*, 347.
- [29] V. S. Afshar, S. C. Warren-Smith, T. M. Monroe, *Opt. Express* **2007**, *15*, 17891.
- [30] S. Afshar, Y. Ruan, S. C. Warren-Smith, T. M. Monroe, *Opt. Lett.* **2008**, *33*, 1473.
- [31] S. C. Warren-Smith, V. S. Afshar, T. M. Monroe, *Opt. Express* **2008**, *16*, 9034.
- [32] A. Autere, H. Jussila, Y. Dai, Y. Wang, H. Lipsanen, Z. Sun, *Adv. Mater.* **2018**, *30*, 1705963.
- [33] V. S. Afshar, T. M. Monroe, C. M. de Sterke, *Opt. Express* **2013**, *21*, 18558.
- [34] S. C. Warren-Smith, J. Wie, M. Chemnitz, R. Kostecki, H. Ebendorff-Heidepriem, T. M. Monroe, M. A. Schmidt, *Opt. Express* **2016**, *24*, 17860.
- [35] S. C. Warren-Smith, M. Chemnitz, H. Schneidewind, R. Kostecki, H. Ebendorff-Heidepriem, T. M. Monroe, M. A. Schmidt, *Opt. Lett.* **2017**, *42*, 1812.
- [36] S. C. Warren-Smith, K. Schaarschmidt, M. Chemnitz, E. P. Schartner, H. Schneidewind, H. Ebendorff-Heidepriem, M. A. Schmidt, *Opt. Lett.* **2019**, *44*, 626.
- [37] N. C. Geib, M. Zilk, T. Pertsch, F. Eilenberger, *Optica* **2019**, *6*, 495.